J Nanopart Res (2017) 19: 385
https://doi.org/10.1007/s11051-017-4075-4

RESEARCH PAPER

Facile fabrication of Ag_3VO_4/attapulgite composites for highly efficient visible light-driven photodegradation towards organic dyes and tetracycline hydrochloride

Yuting Luo · Jie Luo · Guorong Duan · Xiaoheng Liu

Received: 27 May 2017 / Accepted: 16 November 2017 / Published online: 29 November 2017

Abstract An efficient one-dimensional attapulgite (ATP)-based photocatalyst, Ag_3VO_4/ATP nanocomposite, was fabricated by a facile deposition precipitation method with well-dispersed Ag_3VO_4 nanoparticles anchored on the surface of natural ATP fibers. X-ray diffraction (XRD), scanning electron microscopy (SEM), transmission electron microscopy (TEM), Fourier transform infrared spectroscopy (FT-IR), X-ray photoelectron spectroscopy (XPS), and UV-visible diffused reflectance spectroscopy (UV-vis DRS) were employed to investigate the morphologies, structure, and optical property of the prepared photocatalysts. The photocatalytic experiments indicated that the Ag_3VO_4/ATP nanocomposites exhibited enhanced visible light-driven photocatalytic activity towards the degradation of rhodamine B (RhB), methyl orange (MO), and tetracycline hydrochloride (TCH), of which the 20 wt% Ag_3VO_4/ATP sample showed superb photocatalytic performance. As demonstrated by N_2 adsorption-desorption, photocurrent measurements, electrochemical impedance spectroscopy (EIS), and photoluminescence (PL) spectra analyses, the improved photocatalytic activity arose from the enlarged surface area, the facilitated charge transfer, and the suppressed recombination of photogenerated charge carriers in Ag_3VO_4/ATP system. Furthermore, radical scavengers trapping experiments and recycling tests were also conducted. This work gives a new insight into fabrication of highly efficient, stable, and cost-effective visible light-driven photocatalyst for practical application in wastewater treatment and environmental remediation.

Keywords Attapulgite · Ag_3VO_4 · Composites · Photodegradation · Environmental effects

Electronic supplementary material The online version of this article (https://doi.org/10.1007/s11051-017-4075-4) contains supplementary material, which is available to authorized users.

Y. Luo · J. Luo · G. Duan · X. Liu (✉)
Key Laboratory of Education Ministry for Soft Chemistry and Functional Materials, Nanjing University of Science and Technology, Nanjing 210094, China
e-mail: xhliu@njust.edu.cn

Introduction

Stimulated by the global energy crisis and environmental contamination, photocatalysis has attracted tremendous attention during past decades and various photocatalysts, such as metal oxides, metal sulfides, organic compounds, have been utilized in a wide range of photocatalytic fields, including water splitting (Wang et al. 2016), CO_2 reduction (Sun et al. 2016), photocatalytic degradation of organic pollutants (Ma et al. 2013), and organic group transformation (Chen et al. 2016). Among them, TiO_2 is the most widely studied photocatalyst owing to its chemical stability, ready availability, non-toxicity, and high photocatalytic activity (Pozio et al. 2016; Reddy et al. 2015; Reddy et al. 2011). However, the wide band gap of 3.2 eV makes it just responsive to UV light, which limits its practical application in solar light (Wang et al. 2016c). So, it is still urgent to develop visible light-active photocatalysts to satisfy social requirement. In recent years, studies

found that most of the Ag-based semiconductors, such as Ag_3PO_4 (Bi et al. 2011), AgX (X = Br, I) (Wang et al. 2008), Ag_2S (Neelgund and Oki 2011), and Ag_2CrO_4 (Ouyang et al. 2008), could exhibit strong visible light absorption and visible light catalytic activity due to their narrow band gap energy, which showed great potential in the field of photocatalysis. Based on previous reports, monoclinic Ag_3VO_4, as an effective Ag-based photocatalyst with a narrow band gap (2 eV), had exhibited good photocatalytic performance in decomposing organic pollutants and splitting water into H_2 and O_2 (Konta et al. 2003; Ran et al. 2016; Wang et al. 2014). However, the high electron-hole recombination rate and unstability limited its practical application. To the best of our knowledge, much efforts had been strived to coupling Ag_3VO_4 with other co-catalysts to enhance the photocatalytic activity, such as ZnO/Ag_3VO_4 (Kiantazh and Habibi-Yangjeh 2015), $CoFe_2O_4$/Ag/Ag_3VO_4 (Jing et al. 2016), Ag_3VO_4/WO_3 (Yan et al. 2016), and BiOCl/Ag_3VO_4 (Wang et al. 2016a). But as we know, the utilization of natural minerals to enhance the photocatalytic activity of Ag_3VO_4 is rare. Attapulgite (ATP), a kind of hydrated magnesium aluminum natural silicate minerals with a fibrous morphology, has large surface area exhibiting excellent chemical adsorption property, which has been widely applied in the fields of oil drilling, catalysts, chemical sensors, etc. (Cao et al. 2008; Chen et al. 2011; Jin and Chen 2012; Stathatos et al. 2012). Zhang et al. prepared Cu/TiO_2/organo-ATP fiber nanocomposite for the degradation of acetone in air, which showed the optimal photocatalytic activity and 90.35% of acetone was decomposed within 6 h (Zhang et al. 2016a, b). Chen et al. adopted a one-pot hydrothermal carbonization process to synthesize ATP clay@carbon nanocomposite adsorbent with a high adsorption ability for Cr(VI) and Pb(II) ions (Chen et al. 2011). As an economically available raw material, it is of great significance to explore the potentiality to endow these materials with a bright perspective in the wastewater purification.

Here, we adopted a facile deposition precipitation method to fabricate the 0D-1D Ag_3VO_4/ATP nanocomposite photocatalyst for the first time, in which Ag_3VO_4 nanoparticles with an average size of 7 nm distributed on the platform of 1D ATP fibers evenly. With the hybridization of natural ATP, the hybrid nanocomposites showed much better photocatalytic performance than pure Ag_3VO_4 on the photodegradation of rhodamine B (RhB), methyl orange (MO), and tetracycline hydrochloride (TCH) under visible light, which not only decrease the consumption of noble metal, silver, but also remarkably enhance the stability during the recycling runs. The highly efficient, stable, and cost-effective visible light-driven nanocomposite photocatalyst exhibits great potential for wide usage in water treatment.

Materials and methods

Materials used

Silver nitrite ($AgNO_3$) and sodium orthovanadate dodecahydrate ($Na_3VO_4 \cdot 12H_2O$) were purchased from Sinopharm Chemical Reagent Co., Ltd. (PR China). The ATP was obtained from XuYi, Jiangsu, PR China. Deionized water was used for the preparation of all solution. All chemicals were used without further treatment.

Synthesis of photocatalysts

The Ag_3VO_4/ATP nanocomposites with the Ag_3VO_4 loading amount of 10, 20, and 30 wt% were fabricated by a facile deposition precipitation method. In a typical procedure, 0.176 g ATP was dispersed in 150 mL deionized water with sonication for 30 min to get uniformly dispersed suspension. Then 0.4 mmol $AgNO_3$ added for another 10 min sonication to make Ag^+ anchored on the surface of negative charged ATP uniformly. Finally, 20 mL 0.01 M Na_3VO_4 aqueous solution was slowly dropped into the abovementioned mixture with continuously magnetic stirring for another 4 h. The obtained composite was centrifuged, washed with deionized water and ethanol, and dried at 60 °C for 8 h, denoting as 20% Ag_3VO_4/ATP. With the adjustment of the dosage of ATP, 10% Ag_3VO_4/ATP, 30% Ag_3VO_4/ATP, and pure Ag_3VO_4 were also prepared.

Characterization

Powder X-ray diffraction (XRD) analyses were recorded on a D8 Advance diffractometer (Bruker, Germany) at 40 kV and 40 mA with monochromatic high intensity Cu Kα radiation ($\lambda = 1.5418$ Å). Microstructure and morphology information were obtained using a field emission scanning electron microscope (FEI Quanta

250F) at an acceleration voltage of 15.0 kV and a transmission electron microscope (JEOL JEM-2100) with an accelerating voltage of 200 kV. X-ray photoelectron spectroscopy (XPS) was measured on a PHI Quantera II SXM photoelectron spectrometer with a monochromatic Al Kα radiation ($\lambda = 8.4$ Å) as the exciting source to explore the elements of the surface. Functional groups in samples were detected by a Nicolet IS10 Fourier transform infrared spectrometer. The optical properties of the samples were measured using an Evolution 220 UV-vis spectrophotometer (Thermo Fisher, America) from 200 to 800 nm. Solid-state photolumiscence measurements (λ ex = 328 nm) were recorded from 350 to 550 nm on an FL3-TCSPC fluorescence spectrophotometer using 5-nm slit width. The photocurrent measurements were carried out in a standard electrode photoelectrochemical cell using an electrochemical workstation (CHI-660E). The as-prepared sample, platinum wire, and Ag/AgCl were used as the working, counter, and reference electrodes, respectively. 0.5 M sodium sulfate solution was used as the electrolyte.

Photocatalytic experiments

The photocatalytic activity of the as-prepared samples was evaluated by decomposing rhodamine B (10 mg L^{-1}), methyl orange (10 mg L^{-1}), and TCH (50 mg L^{-1}) under visible light irradiation in a photoreaction apparatus. Visible light was generated by a 300-W Xe lamp with a 400-nm cutoff filter to remove light of $\lambda < 400$ nm. 0.4 g/L of each of photocatalyst was added to the aqueous solution of RhB (MO or TCH) in a Pyrex photocatalytic reactor, which was cooled by recycled water to weaken the effect of thermal catalytic. Before illumination, the suspensions were magnetically stirred for 1 h to reach adsorption-desorption equilibrium in the dark. During the adsorption and photoreaction process, at given time intervals of visible light irradiation, about 3 mL of the suspension was collected from each sample and centrifuged to remove catalyst particles. The concentration was analyzed by measuring the maximum absorbance at 553 nm for RhB (464 nm for MO, 357 nm for TCH) using a UV-vis spectrometer (UV-1801). To demonstrate the stability of the Ag_3VO_4/ATP composites, recycling experiment was performed with the photodegradation of RhB under visible light irradiation.

Results and discussion

XRD analysis

The XRD patterns of ATP, Ag_3VO_4, and Ag_3VO_4/ATP nanocomposites with different mass ratios are presented in Fig. 1. For free ATP nanofibers, the diffraction peaks are perfectly indexed as monoclinic ATP (JCPDS No. 21-0958) at 2θ 8.5°, 13.9°, 19.8°, 27.6°, and 35.1°, which correspond to the primary diffraction of the (1 1 0), (2 0 0), (0 4 0), (2 3 1), and (− 1 6 1) planes of ATP. The (110) diffraction peak is ascribed to the basal plane of the ATP structure (Cao et al. 1996). As can be seen from the result, ATP clay exhibits a high degree of crystallinity, in which only quartz impurities exist at $2\theta = 26.7°$. The observed diffraction peaks of pure Ag_3VO_4 nanoparticles in Fig. 1 are completely in accordance with the monoclinic Ag_3VO_4 (JCPDS No. 43-0542). The typical diffraction peaks located at 2θ 19.1°, 30.9°, 32.3°, 35.1°, and 35.9° agree well with the primary reflections of the (011), (− 121), (121), (301), and (202) planes of the Ag_3VO_4, respectively. With the hybridization of ATP, both the main characteristic diffraction peaks of Ag_3VO_4 and ATP have no obvious change and the characteristic peaks of Ag_3VO_4 are predominant, while the intensity of the main peak at $2\theta = 8.5°$ of ATP becomes stronger as the content of ATP increases. It is obvious that the main diffraction peaks of Ag_3VO_4 at 2θ 30.9° and 32.3° become broader; according to the Scherrer equation, the grain size of the Ag_3VO_4/ATP nanocomposites is smaller than that of the bare Ag_3VO_4. Among them, the 20% Ag_3VO_4/ATP

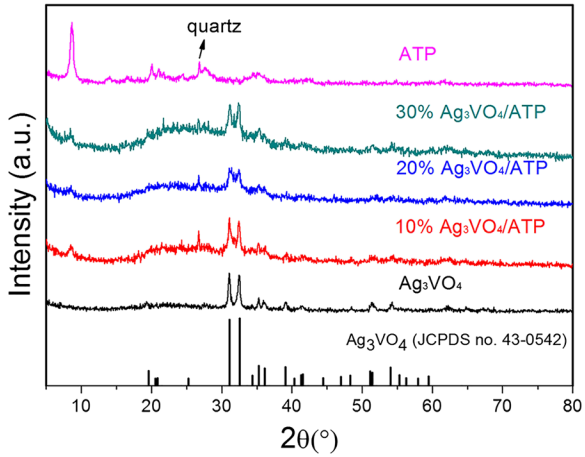

Fig. 1 XRD patterns of ATP, Ag_3VO_4, and Ag_3VO_4/ATP nanocomposites

exhibits the broadest peaks, which indicate the existence of small Ag_3VO_4 nanoparticles. The XRD results verify the co-existence of ATP and Ag_3VO_4 in the Ag_3VO_4/ATP hybrid system.

FT-IR analysis

Figure 2 displays the FT-IR spectra of raw ATP, Ag_3VO_4, and 20% Ag_3VO_4/ATP nanocomposite between 4000 and 500 cm^{-1}. For bare ATP, the band at 3615 cm^{-1} is ascribed to the stretching vibrations of Al-OH-Al groups. The absorption bands located at 3543 and 3363 cm^{-1} are due to the stretching vibration of bound water molecules, including zeolitic water and surface-adsorbed water in ATP (Suárez and García-Romero 2006; Yan et al. 2012). The 1640 cm^{-1} band corresponds to the bending modes of the abovementioned water molecules (Frost et al. 1998; Liu et al. 2012). The band at 1194 cm^{-1} is commonly considered as the exclusive absorbance band of fibrous structure minerals (Sánchez del Río et al. 2009; Xu et al. 2011). Two characteristic absorption peaks located at 1,025,972 cm^{-1} are due to the asymmetric stretching vibration of Si–O bonds while the band at 786 cm^{-1} is ascribed to the symmetric stretching vibration of Si–O–Si bonds (Chang et al. 2009; Tang et al. 2015). Regarding Ag_3VO_4, the peaks at 706 and 850 cm^{-1} are assigned to the symmetry stretching vibration of V–O–V units and V=O double bond vibration, while the peak located at 914 cm^{-1} is ascribed to the VO_3 groups of the VO_4^{3-} tetrahedral (Murugesan et al. 2007). The 1396 cm^{-1} band is according to the Ag–O stretching vibration. Meanwhile, the broad band around 3600 and

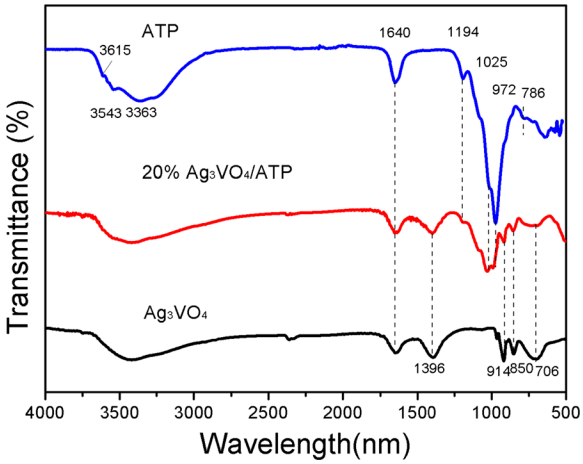

Fig. 2 FTIR spectra of ATP, Ag_3VO_4, and 20% Ag_3VO_4/ATP

1640 cm^{-1} are also ascribed to the adsorbed water molecules. With regard to the spectra of 20% Ag_3VO_4/ATP nanocomposite, both of the main peaks belong to ATP and Ag_3VO_4 can be clearly observed without shift, which is in accordance with the result of XRD. Based on the analysis mentioned above, the conclusion that the Ag_3VO_4/ATP nanocomposite includes both Ag_3VO_4 and ATP can be drawn.

Morphology analysis

To further analyze the microscopic morphology and structure of the samples, the SEM and TEM analyses are performed. As can be seen from Fig. 3a, b, the natural ATP clay exhibits nanorod morphology with a diameter about 40 nm. The surfaces are smooth and the length varies from hundreds of nanometers to several micrometers. Figure 3c is the TEM image of pure Ag_3VO_4. Owing to the huge surface energy, the Ag_3VO_4 nanoparticles aggregate into big size, which reduce the surface area dramatically. From Fig. 3d, e, it is clearly observed that some nanoparticles with diameters approximately 7 nm are dispersed on the fibrous surface of ATP without aggregation in the 20% Ag_3VO_4/ATP sample, which correspond to the Ag_3VO_4 particles. HRTEM image of the 20% Ag3VO_4/ATP sample (Fig. 3f) exhibits the characteristic lattice fringes with crystal plane distances of 0.29, 0.27, and 0.26 nm, which can be indexed to the spacing of the (− 1 2 1), (1 2 1), and (3 0 1) planes in monoclinic Ag_3VO_4. Meanwhile, FESEM, EDS, and elemental mapping images of the 20% Ag_3VO_4/ATP are displayed in Fig. S1. The 20% Ag_3VO_4/ATP sample still keeps the fibrous morphology, indicating the coexistence of Ag_3VO_4 nanoparticles and the fibrous ATP. It is obvious the introduction of ATP has efficiently restricted the aggregation of Ag_3VO_4 naoparticles; at the same time, the small particle will make a big contribution to inhibiting the bulk recombination of the photogenerated charge carriers, thus enhancing the photocatalytic activity.

XPS analysis

XPS measurements are conducted to analyze the surface elements and chemical states of the 20% Ag_3VO_4/ATP composites. Figure 4a shows the survey spectrum of the 20% Ag_3VO_4/ATP composites, which shows the coexistence of Si, Al, Mg, Fe, Ag, V, and O elements without other impurities. The Si, Al, Mg, Fe, and O elements

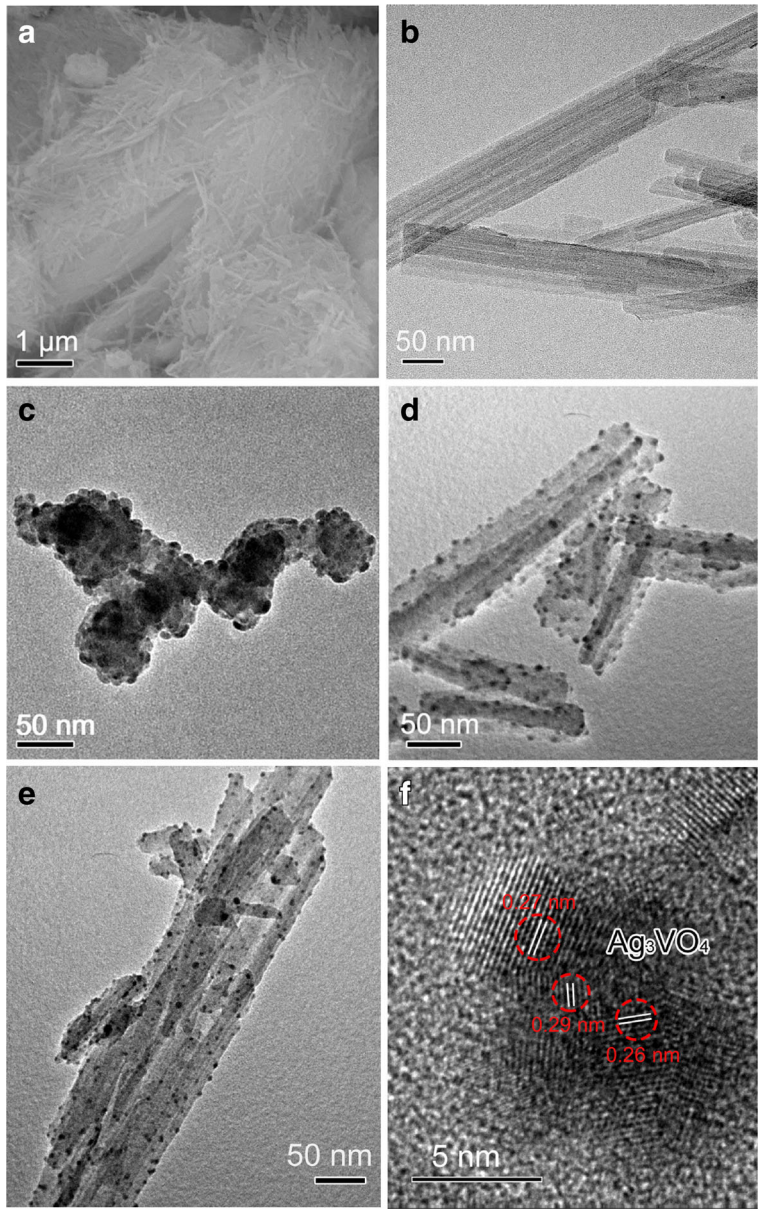

Fig. 3 SEM image of ATP (**a**), TEM images of ATP (**b**), Ag_3VO_4 (**c**), 20% Ag_3VO_4/ATP (**d**, **e**), and HRTEM image of 20% Ag_3VO_4/ATP (**f**)

were derived from the surface of the ATP clay fibers. Figure 4b exhibits two strong peaks at 367.7 and 373.7 eV, which corresponded to $Ag_3d_{5/2}$ and $Ag_3d_{3/2}$. In addition, no peaks have been observed at 369.2 and 375.8 eV, revealing that no Ag^0 was formed during the preparation process (Cao et al. 2012). In Fig. 4c, the peaks at 516.2 and 523.4 eV for the 20% Ag_3VO_4/ATP composite correspond to $V_2p_{3/2}$ and $V_2p_{1/2}$, respectively (Jing et al. 2016). The O_{1s} high-resolution XPS spectrum is shown in Fig. 4d, O 1s peak at 531.7 eV, assigned to O^{2-} in the sample.

Optical properties

To investigate the optical absorption ability of the as-prepared photocatalysts, UV-vis diffuse reflectance spectra were measured as displayed in Fig. 5. It was observed that bare Ag_3VO_4 samples absorbed both ultraviolet and visible light, while ATP was just sensitive to the photons with $\lambda < 450$ nm. For 20% Ag_3VO_4/ATP nanocomposite, the absorption edge prolonged to visible light region exhibiting an obvious red shift compared to pure ATP, which agreed with the color change

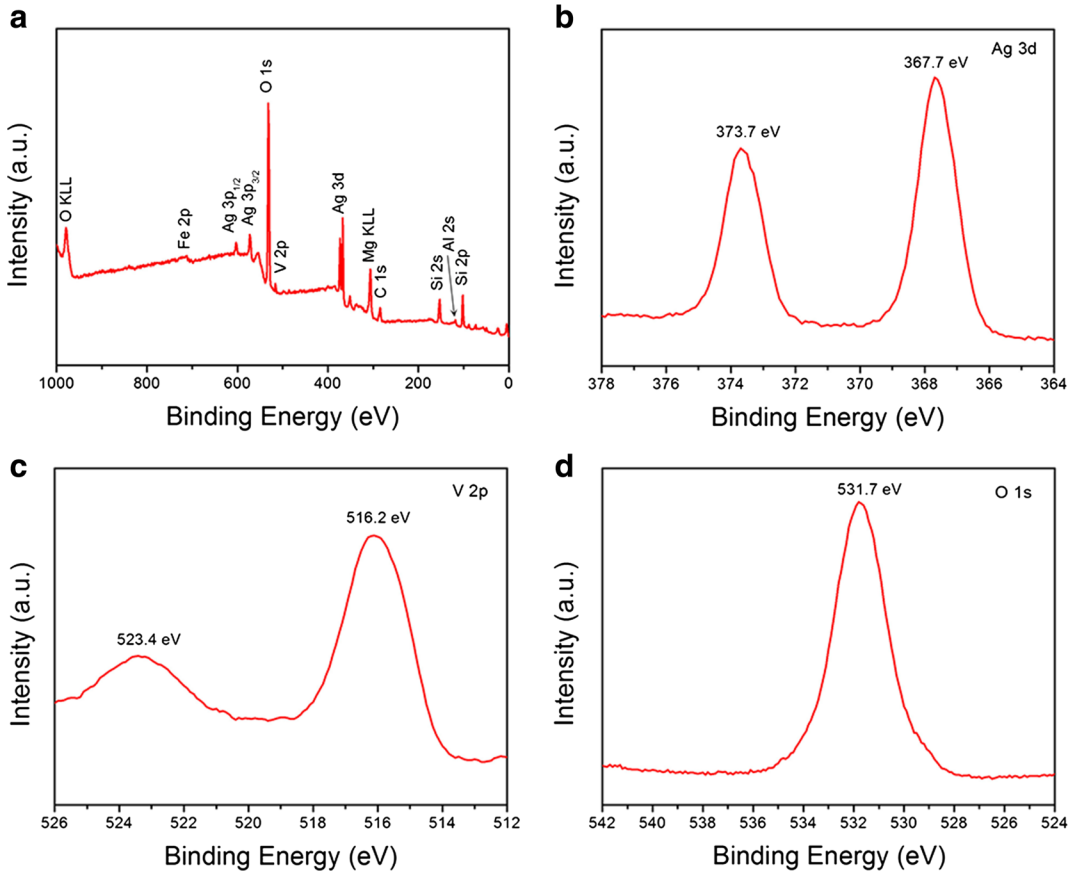

Fig. 4 XPS spectra (**a**) and the high-resolution XPS spectra of Ag 3d (**b**), V 2p (**c**), and O 1s (**d**) of the 20% Ag_3VO_4/ATP nanocomposite

of samples. The optical band gap energies of the samples can be estimated from the diffuse reflection spectra by using the following equation:

$$\alpha h\nu = A\left(h\nu - E_g\right)^{n/2}$$

where α, h, ν, A, and E_g are the absorption coefficient, Planck constant, incident light frequency, constant, and band gap energy, respectively. The value of n describes the type of the transition in a semiconductor, $n = 1$ for direct transition, while $n = 4$ for indirect transition. Therefore, the values of Ag_3VO_4 and ATP are 1 (Zhang et al. 2016a, b; Xu et al. 2010). According to the inset of Fig. 5, the energy band gaps of ATP and Ag_3VO_4 from the plots of $(\alpha h\nu)^2$ versus $h\nu$ can be estimated to be 3.8 and 2 eV, respectively.

N2 adsorption-desorption analysis

The nitrogen adsorption-desorption isotherms of ATP, Ag_3VO_4, and 20% Ag_3VO_4/ATP are displayed in Fig. 6. It can be seen that all these three samples exhibit III isotherms with the hysteresis loop of H3 type, according to the IUPAC classification (Yang et al. 2002). The BET surface areas of ATP, Ag_3VO_4, and 20% Ag_3VO_4/ATP are 121, 10.7, and 185.8 m^2/g, respectively. It is apparent that the introduction of ATP has validly restricted the aggregation of Ag_3VO_4 particles and greatly enhanced the surface area of Ag_3VO_4, thus improving the adsorption property of the nanocomposite photocatalyst and supplying more active sites in the photocatalytic degradation process.

Photocatalytic activity and stability

The environmental issues have attracted much consideration in past decades. Various techniques have been adopted in the water purification, in which the photocatalysis has shown great potential (Chitpong and Husson 2017; Reddy et al. 2016; Reddy et al. 2010; Reddy et al. 2011; Showkat et al. 2007).

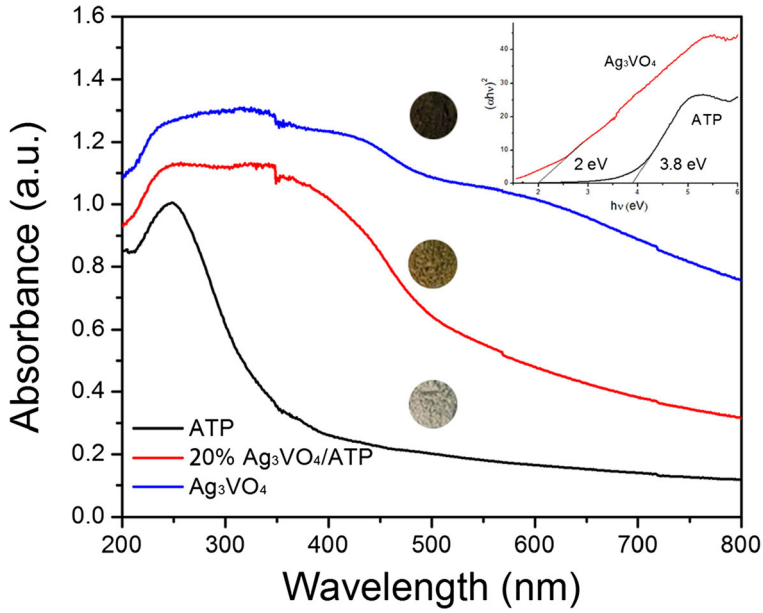

Fig. 5 UV-vis diffuse reflectance spectra of ATP, Ag_3VO_4, and 20% Ag_3VO_4/ATP

Figure 7 exhibits the photocatalytic activity in degradation of RhB, MO, and TCH over Ag_3VO_4/ATP nanocomposites with different contents of Ag_3VO_4 under visible light irradiation. The adsorption-desorption balance has been achieved between the catalyst and organic compounds for 60 min absorption process. From Fig. 7a, c, it can be seen that the photolysis of RhB and MO is negligible without catalysts, indicating that RhB and MO are stable under visible light. The ATP and P25 display good adsorption capacity over the organic dyes, while just exhibit limited photocatalytic activity, which is in accordance with their large specific surface area and the weak absorption capacity of visible light. It is obvious that the photocatalytic performance of Ag_3VO_4/ATP composites is higher than that of pure Ag_3VO_4, which is mainly ascribed to the fast recombination rate of photogenerated charge carriers of pure Ag_3VO_4. For Ag_3VO_4/ATP nanocomposites, the 20-wt% Ag_3VO_4/ATP photocatalyst exhibits the highest photocatalytic activity, which degrades 10 mg/L RhB solution completely in 15 min and decomposes MO solution of 10 mg/L in 80 min under visible light irradiation. What's more, the photocatalytic activity of the mixture of ATP and Ag_3VO_4 with a mass ratio of 4:1 is much lower than the 20% Ag_3VO_4/ATP nanocomposites, which clarified the formation of composites. Obviously, with the addition of ATP, the degradation efficiency improved a lot and the usage of noble metal, silver, has been decreased dramatically. The temporal absorption spectra of RhB solution treated by 20% Ag_3VO_4/ATP are shown in Fig. 7b, in which the absorbance at 554 nm for RhB decreases rapidly. It is noteworthy that the absorption decreases at wavelength of 554 nm for RhB solution accompanied by a blue shift, which had proved to be derived from the formation of a series of *N*-deethylated intermediates of RhB (Hu et al. 2006).

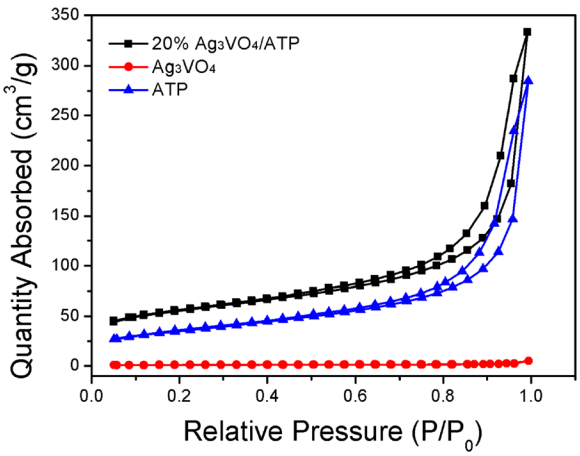

Fig. 6 N_2 sorption-desorption isotherms of ATP, Ag_3VO_4, and 20% Ag_3VO_4/ATP

Tetracycline, as very noted broad-spectrum antibacterial agents, has been widely used in livestock feed and for disease control for several decades (He et al. 2014). However, the non-biodegradation makes it difficult to

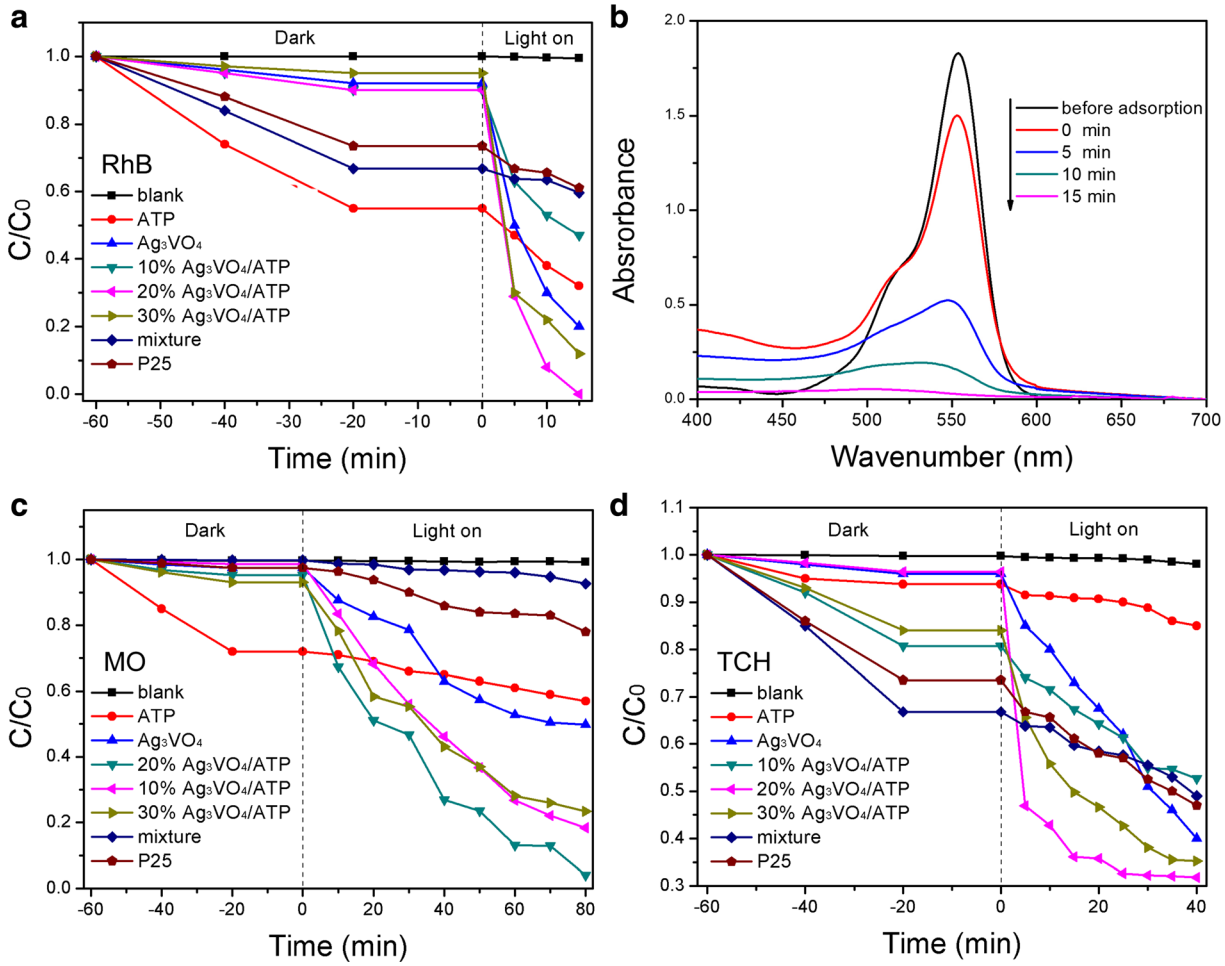

Fig. 7 Photocatalytic degradation of RhB (**a**), MO (**c**), and TCH (**d**) with as-prepared samples; time-dependent UV-vis absorption spectra of RhB solution in the presence of 20% Ag_3VO_4/ATP (**b**)

remove TC from aquatic environments. Both ATP and Ag_3VO_4 have been reported in photocatalytic degradation of TCH (Shi et al. 2016; Yan et al. 2016). Figure 7d displays the photocatalytic degradation of TCH with the as-synthesized samples under visible light irradiation. It is apparent that TCH is stable under visible light while pure ATP and Ag_3VO_4 exhibit low photocatalytic activity in the degradation process. The photocatalytic performance has been efficiently enhanced with the Ag_3VO_4/ATP nanocomposites. Among all the samples, the 20% Ag_3VO_4/ATP sample shows the highest photocatalytic performance, which is in accordance with the photocatalytic degradation process of RhB and MO. Within 40 min irradiation, 70% of TCH has been degraded. From Fig. 7, the content of Ag_3VO_4 has a significant influence on photocatalytic activity. For the 10% Ag_3VO_4/ATP, the content of Ag_3VO_4 is very low, while for the 30% Ag_3VO_4/ATP, the Ag_3VO_4 nanoparticles exhibit an apparent aggregation, as illustrated in Fig. S2. Fig. S3 displays the temporal evolution of the UV-vis spectral variations during TCH degradation over the 20% Ag_3VO_4/ATP sample under visible light irradiation. Obviously, the absorbance at 357 nm decreases rapidly as the time increased, while the absorption peak at 270 nm increases showing a blue shift. This result reveals that some of TCH has been mineralized to small molecules such as CO_2 and H_2O which could absorb UV light (Shi et al. 2016; Wu et al. 2012).

Cycling experiments were performed to investigate the stability and reusability of the 20% Ag_3VO_4/ATP composite over RhB degradation under visible light irradiation, as shown in Fig. 8. After four cycles, the degradation efficiency is still as high as 90%, while Ag_3VO_4 decreased from 90% for the first time to 65% for the fourth time. The

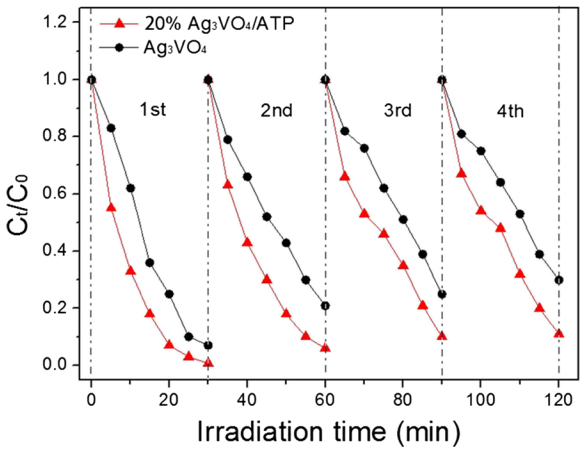

Fig. 8 Four cycling runs of 20% Ag_3VO_4/ATP composite for RhB degradation under visible light irradiation

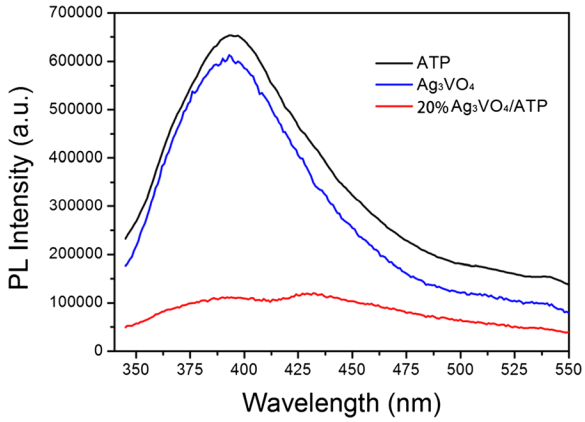

Fig. 10 PL spectra of ATP, Ag_3VO_4, and 20% Ag_3VO_4/ATP

enhanced stability is due to the co-existence of iron, magnesium, and aluminum cations in the ATP, which have been proven to capture excited electrons and efficiently restrain the reduction of Ag^+, thus enhancing the stability of the ATP-based photocatalysts (Luo et al. 2017; Ma et al. 2014). The results demonstrated the high activity and stability of the 20% Ag_3VO_4/ATP nanocomposite for repeated RhB degradation.

The above results confirm that the 20% Ag_3VO_4/ATP composite shows high photocatalytic activity towards colored and colorless pollutants. Especially, it degrades RhB solution of 10 mg/L completely within 15 min and exhibits pretty high stability during the recycling experiments. This work shows that the 20% Ag_3VO_4/ATP composite photocatalyst is high-efficient, stable, and cost-effective, which shows great potential in wastewater treatment and environmental remediation.

Photocurrent and PL analysis

Photocurrent measurement and electrochemical impedance spectroscopy (EIS) were carried out to investigate the photogenerated electron-hole pair separation and transfer efficiency of the obtained photocatalysts, as shown in Fig. 9. The transient photocurrent responses of ATP, Ag_3VO_4, and 20% Ag_3VO_4/ATP were recorded with several on-off cycles of intermittent visible light irradiation. As can be seen in Fig. 9a, it is clear that the photocurrent responses of 20% Ag_3VO_4/ATP were increased significantly compared with that of pure Ag_3VO_4 and ATP, indicating a higher separation efficiency of the photogenerated electron-hole pairs and hence higher photocatalytic activity. The EIS Nyquist plots of ATP, Ag_3VO_4, and 20% Ag_3VO_4/ATP are presented in Fig. 9b. Comparing with ATP and pure Ag_3VO_4, 20% Ag_3VO_4/ATP exhibited much smaller

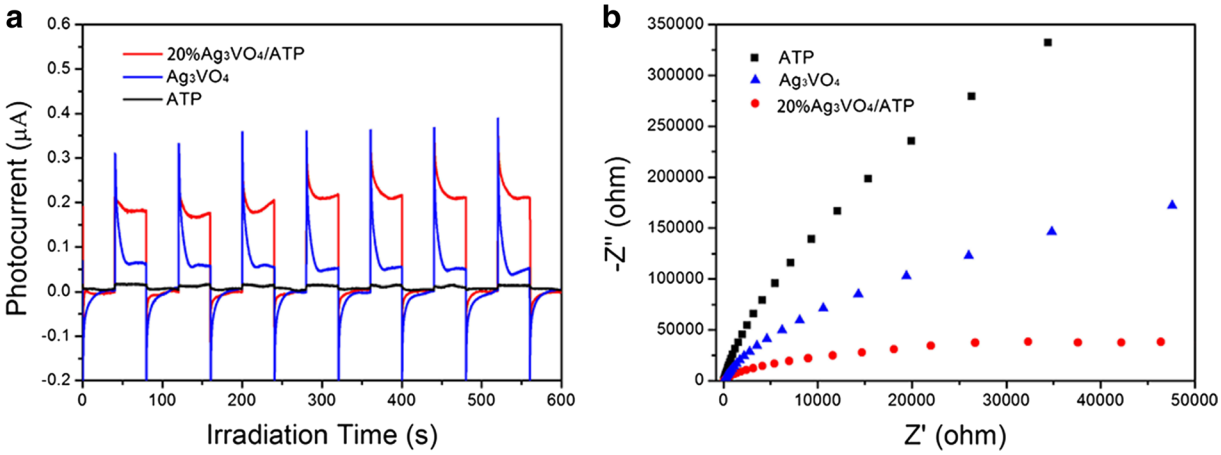

Fig. 9 **a** Transient photocurrent response and **b** Nyquist plots of EIS for ATP, Ag_3VO_4, and 20% Ag_3VO_4/ATP

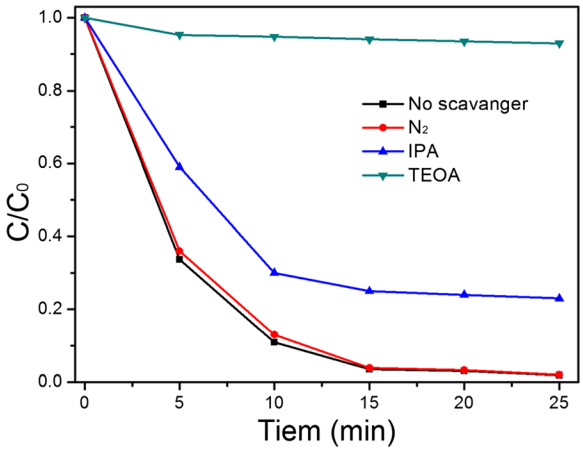

Fig. 11 Trapping experiment of active species during the photocatalytic degradation of RhB over 20% Ag_3VO_4/ATP sample under visible light irradiation

semicircles, revealing a dramatic decrease of charge transfer resistance in the 20% Ag_3VO_4/ATP composite.

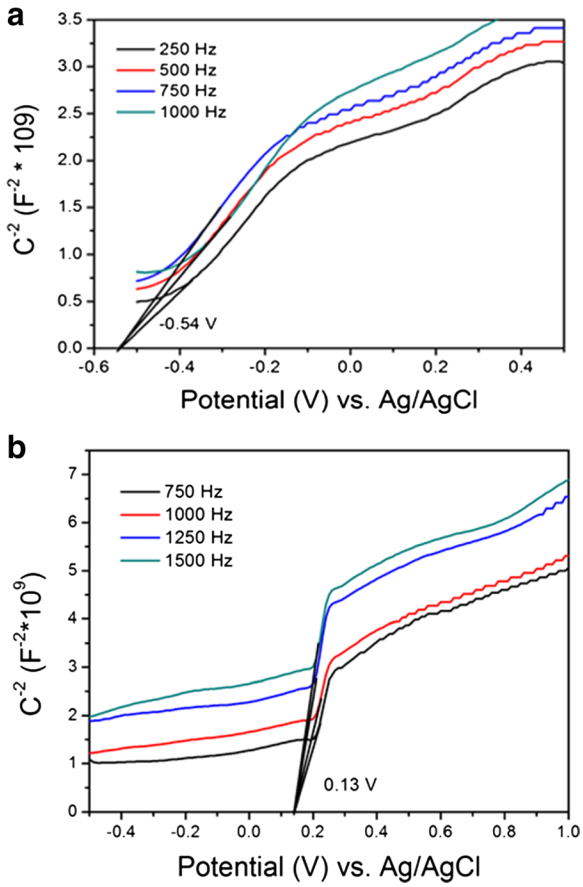

Fig. 12 Mott–Schottky plots of **a** pure ATP and **b** Ag_3VO_4

The photoluminescence spectra were employed to further study the photogenerated electron-hole pair transfer and separation properties of the system (Liqiang et al. 2006). The relative spectra are exhibited in Fig. 10 under the excitation wavelength of 328 nm. Obviously, the emission intensity of Ag_3VO_4 significantly decreased after the hybridization of ATP, implying that the recombination efficiency of photogenerated electron-hole pairs in 20% Ag_3VO_4/ATP was greatly inhibited.

Possible photocatalytic mechanism

In order to explore the photocatalytic mechanism of RhB degradation, various trapping experiments were conducted. The results of the introduction of different radical scavengers during the degradation of RhB over the 20% Ag_3VO_4/ATP photocatalysts under visible light irradiation are depicted in Fig. 11 (Li et al. 2016; Shan et al. 2016). When TEOA (a hole radical (h^+) quencher) was added into the photocatalytic system, the photodegradation efficiency was decreased remarkably compared to the reaction without radical scavengers, indicating that the photogenerated holes were the predominant active species during the photodegradation process. By contrast, when the controlled experiment was conducted under the N_2 atmosphere, the RhB degradation was close to the reaction in the absence of radical scavengers, suggesting that $\cdot O_2^-$ made very small contribution to the photocatalytic reaction. Furthermore, with the addition of IPA (a hydroxyl radical ($\cdot$OH) quencher), the degradation rates of RhB decreased from 100 to 80%. Thus, the results explicitly indicated that the photodegradation of RhB over the 20-wt% Ag_3VO_4/ATP mainly occurred through the synergetic effect of h^+ and $\cdot$OH.

Furthermore, on the basis of the results of Mott–Schottky plots, as shown in Fig. 12, the flat-band potentials (E_{fb}) were estimated to be − 0.54 V for ATP and 0.13 V for Ag_3VO_4 (Gelderman et al. 2007). When Ag/AgCl electrode was used as a reference electrode, the conduction band potentials of ATP and Ag_3VO_4 were approximately located at − 0.34 and 0.33 V, respectively. Moreover, by analyzing these data combined with the band gap values obtained from the UV-vis diffuse reflectance spectra, the VB potential of ATP and Ag_3VO_4 could be calculated to be 3.46 and 2.33 V. Apparently, the CB level of Ag_3VO_4 is less negative than the redox potential of $\cdot O_2^-/O_2$ (ca. − 0.33 V), so it is difficult to

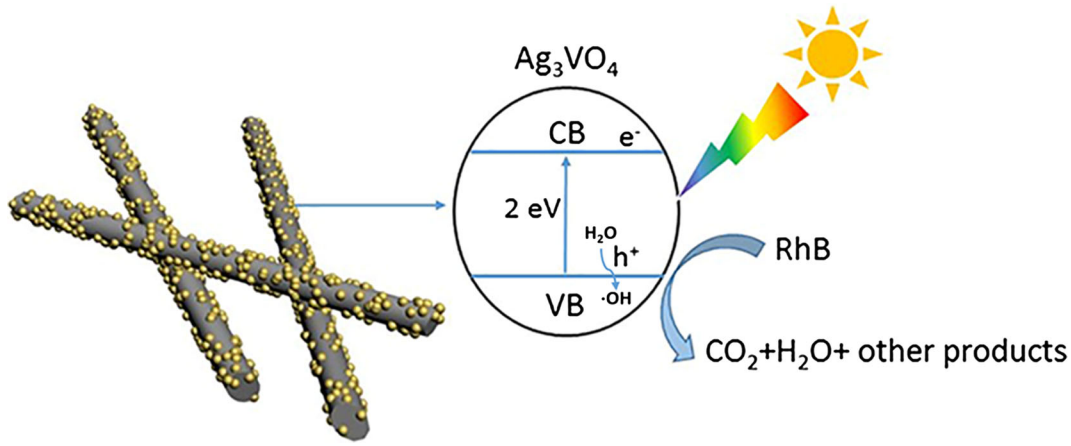

Fig. 13 Schematic diagram of the photocatalytic degradation of RhB over the 20% Ag_3VO_4/ATP photocatalyst

reduce absorbed O_2 to produce $^{\cdot}O_2^-$ in the photodegradation process (Deng et al. 2016; Hong et al. 2016). The results are in good agreement with the trapping experiments. A possible mechanism was proposed for the degradation of RhB over 20-wt% Ag_3VO_4/ATP, as illustrated in Fig. 13. The small Ag_3VO_4 nanoparticles were deposited on the platform of the ATP nanofibers. Under visible light irradiation, Ag_3VO_4 nanoparticles were excited to generate e^- and h^+, and the holes could directly affect the organic compounds to produce CO_2, H_2O, and other products. Meanwhile, the h^+ could also oxide H_2O to generate $^{\cdot}OH$ radicals, which could effectively decompose organics as well.

Conclusion

In this work, the natural one-dimensional ATP clay was used as a carrier for Ag_3VO_4 nanoparticles, and the resultant Ag_3VO_4/ATP hybrid photocatalyst exhibited enhanced photocatalytic activity and stability both in the degradation of azo dyes, RhB and MO, and antibiotic, TCH, of which the 20 wt% Ag_3VO_4/ATP nanocomposite displayed optimal photocatalytic performance under visible light irradiation. The synergistic effect, strong light absorption ability, fast transfer, and valid separation of electron-hole pairs were beneficial for the improved photocatalytic activity. This work provides a plausible strategy to design high-efficiency, low cost, and extremely stable photocatalysts for the wastewater treatment and environmental remediation.

Funding information This work was supported by the National Natural Science Foundation of China (grant nos. 51572126 and 51372118) and the Department of Education of Jiangsu Province (KYLX_0352).

Compliance with ethical standards

Conflict of interest The authors declare that they have no conflict of interest.

References

Bi Y, Ouyang S, Umezawa N, Cao J, Ye J (2011) Facet effect of single-crystalline Ag_3PO_4 sub-microcrystals on photocatalytic properties. J Am Chem Soc 133(17):6490–6492. https://doi.org/10.1021/ja2002132

Cao E, Bryant R, Williams DJA (1996) Electrochemical properties of Na–attapulgite. J Colloid Interf Sci 179(1):143–150. https://doi.org/10.1006/jcis.1996.0196

Cao JL, Shao GS, Wang Y, Liu Y, Yuan ZY (2008) CuO catalysts supported on attapulgite clay for low-temperature CO oxidation. Catal Commun 9(15):2555–2559. https://doi.org/10.1016/j.catcom.2008.07.016

Cao J, Luo B, Lin H, Xu B, Chen S (2012) Visible light photocatalytic activity enhancement and mechanism of AgBr/Ag_3PO_4 hybrids for degradation of methyl orange. J Hazard Mater 217–218:107–115. https://doi.org/10.1016/j.jhazmat.2012.03.002

Chang P-H, Li Z, Yu TL, Munkhbayer S, Kuo TH, Hung YC, Jean JS, Lin KH (2009) Sorptive removal of tetracycline from water by palygorskite. J Hazard Mater 165(1-3):148–155. https://doi.org/10.1016/j.jhazmat.2008.09.113

Chen LF, Liang HW, Lu Y, Cui CH, Yu SH (2011) Synthesis of an attapulgite clay@carbon nanocomposite adsorbent by a hydrothermal carbonization process and their application in the

removal of toxic metal ions from water. Langmuir 27(14): 8998–9004. https://doi.org/10.1021/la2017165

Chen W, Liu T-Y, Huang T, Liu X-H, Yang X-J (2016) Novel mesoporous P-doped graphitic carbon nitride nanosheets coupled with $ZnIn_2S_4$ nanosheets as efficient visible light driven heterostructures with remarkably enhanced photoreduction activity. Nano 8(6):3711–3719. https://doi.org/10.1039/C5NR07695A

Chitpong N, Husson SM (2017) Polyacid functionalized cellulose nanofiber membranes for removal of heavy metals from impaired waters. J Membr Sci 523:418–429. https://doi.org/10.1016/j.memsci.2016.10.020

Deng Y, Tang L, Zeng G, Wang J, Zhou Y, Wang J, Tang J, Liu Y, Peng B, Chen F (2016) Facile fabrication of a direct Z-scheme Ag_2CrO_4/g-C_3N_4 photocatalyst with enhanced visible light photocatalytic activity. J Mol Catal A Chem 421: 209–221. https://doi.org/10.1016/j.molcata.2016.05.024

Frost RL, Cash GA, Kloprogge JT (1998) 'Rocky Mountain leather', sepiolite and attapulgite—an infrared emission spectroscopic study. Vib Spectrosc 16(2):173–184. https://doi.org/10.1016/S0924-2031(98)00014-9

Gelderman K, Lee L, Donne SW (2007) Flat-band potential of a semiconductor: using the Mott–Schottky equation. J Chem Educ 84(4):685. https://doi.org/10.1021/ed084p685

He D, Sun Y, Xin L, Feng J (2014) Aqueous tetracycline degradation by non-thermal plasma combined with nano-TiO_2. Chem Eng J 258:18–25. https://doi.org/10.1016/j.cej.2014.07.089

Hong Y, Jiang Y, Li C, Fan W, Yan X, Yan M, Shi W (2016) In-situ synthesis of direct solid-state Z-scheme V_2O_5/g-C_3N_4 heterojunctions with enhanced visible light efficiency in photocatalytic degradation of pollutants. Appl Catal B Environ 180:663–673. https://doi.org/10.1016/j.apcatb.2015.06.057

Hu X, Mohamood T, Ma W, Chen C, Zhao J (2006) Oxidative decomposition of rhodamine B dye in the presence of VO_2^+ and/or Pt(IV) under visible light irradiation: N-deethylation, chromophore cleavage, and mineralization. J Phys Chem B 110(51):26012–26018. https://doi.org/10.1021/jp063588q

Jin L, Chen D (2012) Enhancement in photovoltaic performance of phthalocyanine-sensitized solar cells by attapulgite nanoparticles. Electrochim Acta 72:40–45. https://doi.org/10.1016/j.electacta.2012.03.167

Jing L, Xu Y, Huang S, Xie M, He M, Xu H, Li H, Zhang Q (2016) Novel magnetic $CoFe_2O_4$/Ag/Ag_3VO_4 composites: highly efficient visible light photocatalytic and antibacterial activity. Appl Catal B Environ 199:11–22. https://doi.org/10.1016/j.apcatb.2016.05.049

Kiantazh F, Habibi-Yangjeh A (2015) Ag_3VO_4/ZnO nanocomposites with an n–n heterojunction as novel visible-light-driven photocatalysts with highly enhanced activity. Mater Sci Semicond Process 39:671–679. https://doi.org/10.1016/j.mssp.2015.06.011

Konta R, Kato H, Kobayashi H, Kudo A (2003) Photophysical properties and photocatalytic activities under visible light irradiation of silver vanadates. Phys Chem Chem Phys 5(14):3061. https://doi.org/10.1039/b300179b

Li Y, Jin R, Fang X, Yang Y, Yang M, Liu X, Xing Y, Song S (2016) In situ loading of Ag_2WO_4 on ultrathin g-C_3N_4 nanosheets with highly enhanced photocatalytic performance. J Hazard Mater 313:219–228. https://doi.org/10.1016/j.jhazmat.2016.04.011

Liqiang J, Yichun Q, Baiqi W, Shudan L, Baojiang J, Libin Y, Wei F, Honggang F, Jiazhong S (2006) Review of photoluminescence performance of nano-sized semiconductor materials and its relationships with photocatalytic activity. Sol Energy Mater Sol Cells 90(12):1773–1787. https://doi.org/10.1016/j.solmat.2005.11.007

Liu Q, Yao X, Cheng H, Frost RL (2012) An infrared spectroscopic comparison of four Chinese palygorskites. Spectrochim Acta A Mol Biomol Spectrosc 96:784–789. https://doi.org/10.1016/j.saa.2012.07.025

Luo J, Duan G, Wang W, Luo Y, Liu X (2017) Size-controlled synthesis of palygorskite/Ag_3PO_4 nanocomposites with enhanced visible-light photocatalytic performance. Appl Clay Sci 143:273–278. https://doi.org/10.1016/j.clay.2017.04.004

Ma J, Zou J, Li L, Yao C, Zhang T, Li D (2013) Synthesis and characterization of Ag_3PO_4 immobilized in bentonite for the sunlight-driven degradation of Orange II. Appl Catal B Environ 134–135:1–6. https://doi.org/10.1016/j.apcatb.2012.12.032

Ma JF, Zhou J, Li LY, Yao C, Kong Y, Cui BY, Zhu RL, Li DL (2014) Nanocomposite of attapulgite-Ag_3PO_4 for Orange II photodegradation. Appl Catal B Environ 144:36–40. https://doi.org/10.1016/j.apcatb.2013.06.029

Murugesan S, Wijayasinghe A, Bergman B (2007) Preparation and characterization of CuI-doped silver borovanadate superionic system. Solid State Ionics 178(11-12):779–783. https://doi.org/10.1016/j.ssi.2007.02.025

Neelgund GM, Oki A (2011) Photocatalytic activity of CdS and Ag_2S quantum dots deposited on poly(amidoamine) functionalized carbon nanotubes. Appl Catal B Environ 110:99–107. https://doi.org/10.1016/j.apcatb.2011.08.031

Ouyang S, Li Z, Ouyang Z, Yu T, Ye J, Zou Z (2008) Correlation of crystal structures, electronic structures, and photocatalytic properties in a series of ag-based oxides: $AgAlO_2$, $AgCrO_2$, and Ag_2CrO_4. J Phys Chem C 112(8):3134–3141. https://doi.org/10.1021/jp077127w

Pozio A, Masci A, Pasquali M (2016) Nickel-TiO_2 nanotube anode for photo-electrolysers. Sol Energy 136:590–596. https://doi.org/10.1016/j.solener.2016.07.040

Ran R, McEvoy JG, Zhang Z (2016) Ag_2O/Ag_3VO_4/$Ag_4V_2O_7$ heterogeneous photocatalyst prepared by a facile hydrothermal synthesis with enhanced photocatalytic performance under visible light irradiation. Mater Res Bull 74:140–150. https://doi.org/10.1016/j.materresbull.2015.08.028

Reddy KR, Nakata K, Ochiai T, Murakami T, Tryk DA, Fujishima A (2010) Nanofibrous TiO_2-core/conjugated polymer-sheath composites: synthesis, structural properties and photocatalytic activity. J Nanosci Nanotechnol 10(12):7951–7957. https://doi.org/10.1166/jnn.2010.3143

Reddy KR, Nakata K, Ochiai T, Murakami T, Tryk DA, Fujishima A (2011) Facile fabrication and photocatalytic application of ag nanoparticles-TiO_2 nanofiber composites. J Nanosci Nanotechnol 11(4):3692–3695. https://doi.org/10.1166/jnn.2011.3805

Reddy KR, Hassan M, Gomes VG (2015) Hybrid nanostructures based on titanium dioxide for enhanced photocatalysis. Appl Catal A Gen 489:1–16. https://doi.org/10.1016/j.apcata.2014.10.001

Reddy KR, Karthik KV, Prasad SBB, Soni SK, Jeong HM, Raghu AV (2016) Enhanced photocatalytic activity of nanostructured titanium dioxide/polyaniline hybrid photocatalysts.

Polyhedron 120:169–174. https://doi.org/10.1016/j.poly.2016.08.029

Sánchez del Río M, Boccaleri E, Milanesio M, Croce G, van Beek W, Tsiantos C, Chyssikos GD, Gionis V, Kacandes GH, Suárez M, García-Romero E (2009) A combined synchrotron powder diffraction and vibrational study of the thermal treatment of palygorskite–indigo to produce Maya blue. J Mater Sci 44(20):5524–5536. https://doi.org/10.1007/s10853-009-3772-5

Shan W, Hu Y, Bai Z, Zheng M, Wei C (2016) In situ preparation of g-C_3N_4/bismuth-based oxide nanocomposites with enhanced photocatalytic activity. Appl Catal B Environ 188: 1–12. https://doi.org/10.1016/j.apcatb.2016.01.058

Shi Y, Yang Z, Wang B, An H, Chen Z, Cui H (2016) Adsorption and photocatalytic degradation of tetracycline hydrochloride using a palygorskite-supported Cu_2O–TiO_2 composite. Appl Clay Sci 119(Part 2):311–320. https://doi.org/10.1016/j.clay.2015.10.033

Showkat AM et al (2007) Analysis of heavy metal toxic ions by adsorption onto amino-functionalized ordered mesoporous silica, vol 28, 11. Korean Chemical Society, Seoul

Stathatos E, Papoulis D, Aggelopoulos CA, Panagiotaras D, Nikolopoulou A (2012) TiO_2/palygorskite composite nanocrystalline films prepared by surfactant templating route: synergistic effect to the photocatalytic degradation of an azo-dye in water. J Hazard Mater 211–212:68–76. https://doi.org/10.1016/j.jhazmat.2011.11.055

Suárez M, García-Romero E (2006) FTIR spectroscopic study of palygorskite: influence of the composition of the octahedral sheet. Appl Clay Sci 31(1-2):154–163. https://doi.org/10.1016/j.clay.2005.10.005

Sun W, Qian C, He L, Ghuman KK, Wong APY, Jia J, Jelle AA, O'Brien PG, Reyes LM, Wood TE, Helmy AS, Mims CA, Singh CV, Ozin GA (2016) Heterogeneous reduction of carbon dioxide by hydride-terminated silicon nanocrystals. Nat Commun 7:12553. https://doi.org/10.1038/ncomms12553 http://www.nature.com/articles/ncomms12553#supplementary-information

Tang J, Mu B, Zong L, Zheng M, Wang A (2015) Fabrication of attapulgite/carbon composites from spent bleaching earth for the efficient adsorption of methylene blue. RSC Adv 5(48): 38443–38451. https://doi.org/10.1039/C5RA02497H

Wang P, Huang B, Qin X, Zhang X, Dai Y, Wei J, Whangbo M-H (2008) Ag@AgCl: a highly efficient and stable photocatalyst active under visible light. Angew Chem Int Ed 47(41):7931–7933. https://doi.org/10.1002/anie.200802483

Wang J, Yang X, Chen J, Xian J, Meng S, Zheng Y, Shao Y, Li D (2014) Photocatalytic activity of novel $Ag_4V_2O_7$ photocatalyst under visible light irradiation. J Am Ceram Soc 97(1):267–274. https://doi.org/10.1111/jace.12639

Wang P, Tang H, Ao Y, Wang C, Hou J, Qian J, Li Y (2016a) In-situ growth of Ag_3VO_4 nanoparticles onto BiOCl nanosheet to form a heterojunction photocatalyst with enhanced performance under visible light irradiation. J Alloys Compd 688(Part B):1–7. https://doi.org/10.1016/j.jallcom.2016.07.180

Wang Q, Hisatomi T, Jia Q, Tokudome H, Zhong M, Wang C, Pan Z, Takata T, Nakabayashi M, Shibata N, Li Y, Sharp ID, Kudo A, Yamada T, Domen K (2016) Scalable water splitting on particulate photocatalyst sheets with a solar-to-hydrogen energy conversion efficiency exceeding 1%. Nat Mater 15(6):611–615. https://doi.org/10.1038/nmat4589. http://www.nature.com/nmat/journal/v15/n6/abs/nmat4589.html#supplementary-information

Wang X, Li T, Yu R, Yu H, Yu J (2016b) Highly efficient TiO_2 single-crystal photocatalyst with spatially separated Ag and F- bi-cocatalysts: orientation transfer of photogenerated charges and their rapid interfacial reaction. J Mater Chem A 4(22):8682–8689. https://doi.org/10.1039/C6TA02039A

Wu J, Zhang H, Oturan N, Wang Y, Chen L, Oturan MA (2012) Application of response surface methodology to the removal of the antibiotic tetracycline by electrochemical process using carbon-felt cathode and DSA (Ti/RuO_2–IrO_2) anode. Chemosphere 87(6):614–620. https://doi.org/10.1016/j.chemosphere.2012.01.036

Xu H, Li H, Sun G, Xia J, Wu C, Ye Z, Zhang Q (2010) Photocatalytic activity of La_2O_3-modified silver vanadates catalyst for rhodamine B dye degradation under visible light irradiation. Chem Eng J 160(1):33–41. https://doi.org/10.1016/j.cej.2010.02.054

Xu J, Zhang J, Wang Q, Wang A (2011) Disaggregation of palygorskite crystal bundles via high-pressure homogenization. Appl Clay Sci 54(1):118–123. https://doi.org/10.1016/j.clay.2011.07.020

Yan W, Liu D, Tan D, Yuan P, Chen M (2012) FTIR spectroscopy study of the structure changes of palygorskite under heating. Spectrochim Acta A Mol Biomol Spectrosc 97:1052–1057. https://doi.org/10.1016/j.saa.2012.07.085

Yan M, Wu Y, Zhu F, Hua Y, Shi W (2016) The fabrication of a novel Ag_3VO_4/WO_3 heterojunction with enhanced visible light efficiency in the photocatalytic degradation of TC. Phys Chem Chem Phys 18(4):3308–3315. https://doi.org/10.1039/C5CP05599G

Yang J, Li D, Wang X, Yang X, Lu L (2002) Rapid synthesis of nanocrystalline TiO_2/SnO_2 binary oxides and their photoinduced decomposition of methyl orange. J Solid State Chem 165(1):193–198. https://doi.org/10.1006/jssc.2001.9526

Zhang J, Chen A, Wang L, Li X'a, Huang W (2016a) Striving toward visible light photocatalytic water splitting based on natural silicate clay mineral: the interface modification of attapulgite at the atomic-molecular level. ACS Sustain Chem Eng 4(9):4601–4607. https://doi.org/10.1021/acssuschemeng.6b00716

Zhang G, Wang H, Guo S, Wang J, Liu J (2016b) Synthesis of Cu/TiO_2/organo-attapulgite fiber nanocomposite and its photocatalytic activity for degradation of acetone in air. Appl Surf Sci 362:257–264. https://doi.org/10.1016/j.apsusc.2015.11.218